iScience

CellPress

Article

High Precision of Spike Timing across Olfactory Receptor Neurons Allows Rapid Odor Coding in *Drosophila*

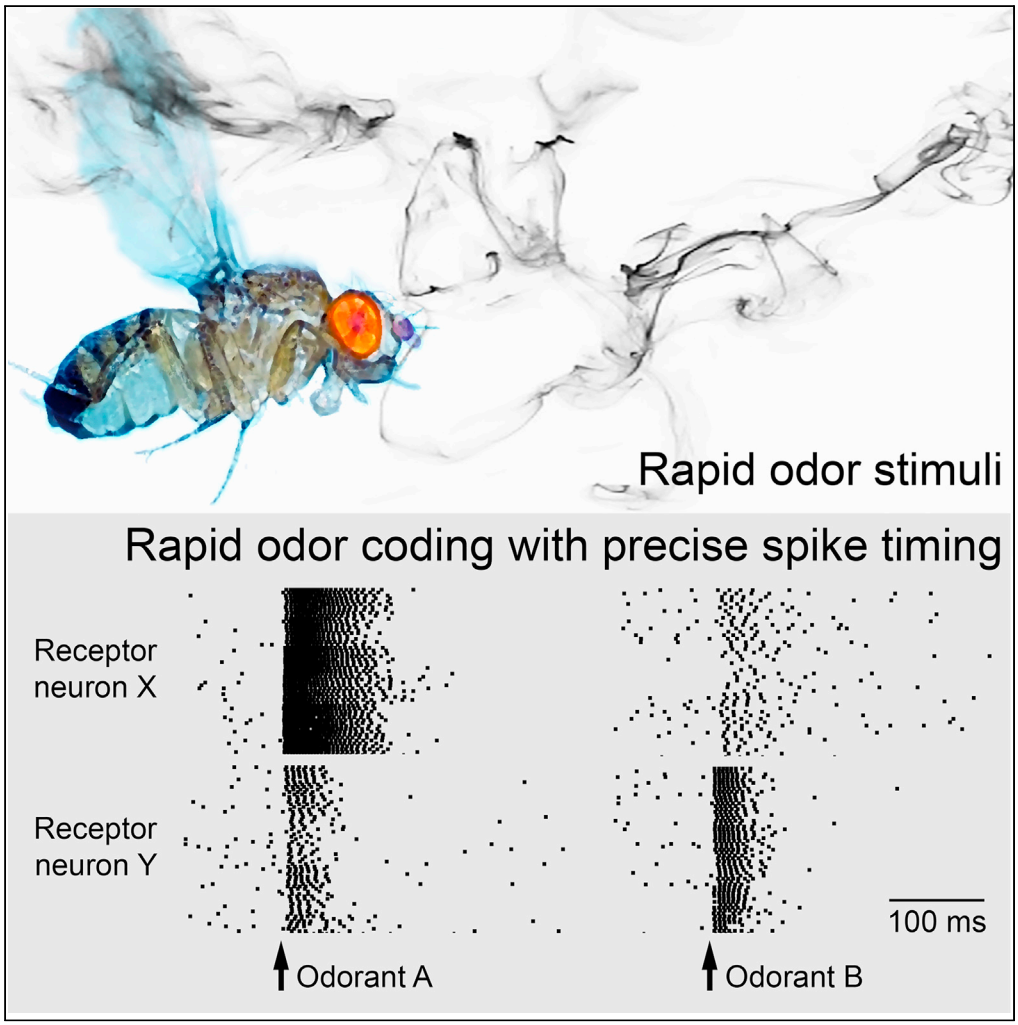

Alexander Egea-Weiss, Alpha Renner, Christoph J. Kleineidam, Paul Szyszka

paul.szyszka@uni-konstanz.de

HIGHLIGHTS

Olfactory receptor neuron responses are fast and temporally precise

Odor-evoked spikes can occur 3 ms after odorant arrival and jitter less than 1 ms

First-spike timing varies over a wider concentration range than spike rate

Neural network model demonstrates the plausibility of a spike-timing code for odors

Egea-Weiss et al., iScience 4, 76–83
June 29, 2018
https://doi.org/10.1016/j.isci.2018.05.009

iScience

CellPress

Article

High Precision of Spike Timing across Olfactory Receptor Neurons Allows Rapid Odor Coding in *Drosophila*

Alexander Egea-Weiss,[1,3] Alpha Renner,[1,2,3] Christoph J. Kleineidam,[1] and Paul Szyszka[1,4,*]

SUMMARY

In recent years, it has become evident that olfaction is a fast sense, and millisecond short differences in stimulus onsets are used by animals to analyze their olfactory environment. In contrast, olfactory receptor neurons are thought to be relatively slow and temporally imprecise. These observations have led to a conundrum: how, then, can an animal resolve fast stimulus dynamics and smell with high temporal acuity? Using parallel recordings from olfactory receptor neurons in *Drosophila*, we found hitherto unknown fast and temporally precise odorant-evoked spike responses, with first spike latencies (relative to odorant arrival) down to 3 ms and with a SD below 1 ms. These data provide new upper bounds for the speed of olfactory processing and suggest that the insect olfactory system could use the precise spike timing for olfactory coding and computation, which can explain insects' rapid processing of temporal stimuli when encountering turbulent odor plumes.

INTRODUCTION

Olfaction is a highly dynamic process, as wind and self-generated movement expose olfactory organs to rapid changes in odorant concentrations (Celani et al., 2014; Farrell et al., 2002; Huston et al., 2015; Murlis, 1992; van Breugel and Dickinson, 2014; Vickers, 2000). Flying insects are particularly well adapted for rapidly detecting and tracking odorants in turbulent environments. *Drosophila*, for example, can react within 70 ms after the response onset of olfactory receptor neurons (Gaudry et al., 2013), and moths and honey bees use millisecond short differences in odorant arrival for odor source separation (Baker et al., 1998; Szyszka et al., 2012). These fast smelling capabilities imply a rapid neural coding mechanism for odors. The speed at which sensory systems can encode stimuli depends on the temporal precision of stimulus-evoked spikes: Higher temporal precision allows faster stimulus encoding, because postsynaptic neurons require shorter integration times to separate stimulus-evoked spikes from spontaneous spikes (Jeanne and Wilson, 2015; Thorpe et al., 2001). Accordingly, many sensory systems use millisecond or even sub-millisecond precise spike timing across sensory neurons to rapidly encode stimulus features (e.g., visual patterns in salamanders [Gollisch and Meister, 2008], direction of sound in barn owls [Carr and Konishi, 1990], and touch location in leeches [Thomson and Kristan, 2006]).

Odorant identity is encoded in the differences of spike rates and spike latencies across olfactory receptor neuron types (insects [de Bruyne et al., 1999; Martelli et al., 2013; Schneider et al., 1964]; vertebrates [Duchamp-Viret et al., 1999; Getchell and Shepherd, 1978]). However, the speed and the temporal precision of stimulus-evoked spikes in olfactory receptor neurons have not yet been accurately determined. Using parallel recordings from olfactory receptor neurons in *Drosophila*, we found fast and temporally precise odorant-evoked spike responses: The first odorant-evoked spike occurred with a short latency down to 3 ms and with a trial-to-trial and neuron-to-neuron SD (jitter) below 1 ms. Using a simple neural network model, we demonstrate the plausibility of a rank order code for odorant identity based on relative spike latencies across different receptor neuron types.

RESULTS AND DISCUSSION

To determine the speed and temporal precision of odorant-evoked spikes in olfactory receptor neurons, we recorded from pairs of *Drosophila* olfactory receptor neurons that express the same olfactory receptor (neurons expressing the receptor OR59b and neurons expressing OR22a, Figure 1A; original data are available in Data S1). To mimic the intermittent and rapid odorant stimuli that insects encounter when flying through an odor plume (Celani et al., 2014; Farrell et al., 2002; Huston et al., 2015; Murlis, 1992; Riffell

[1]University of Konstanz, Department of Biology, Neurobiology, Konstanz 78457, Germany

[2]Institute of Neuroinformatics, University of Zurich and ETH Zurich, Zürich 8057, Switzerland

[3]These authors contributed equally

[4]Lead Contact

*Correspondence: paul.szyszka@uni-konstanz.de

https://doi.org/10.1016/j.isci.2018.05.009

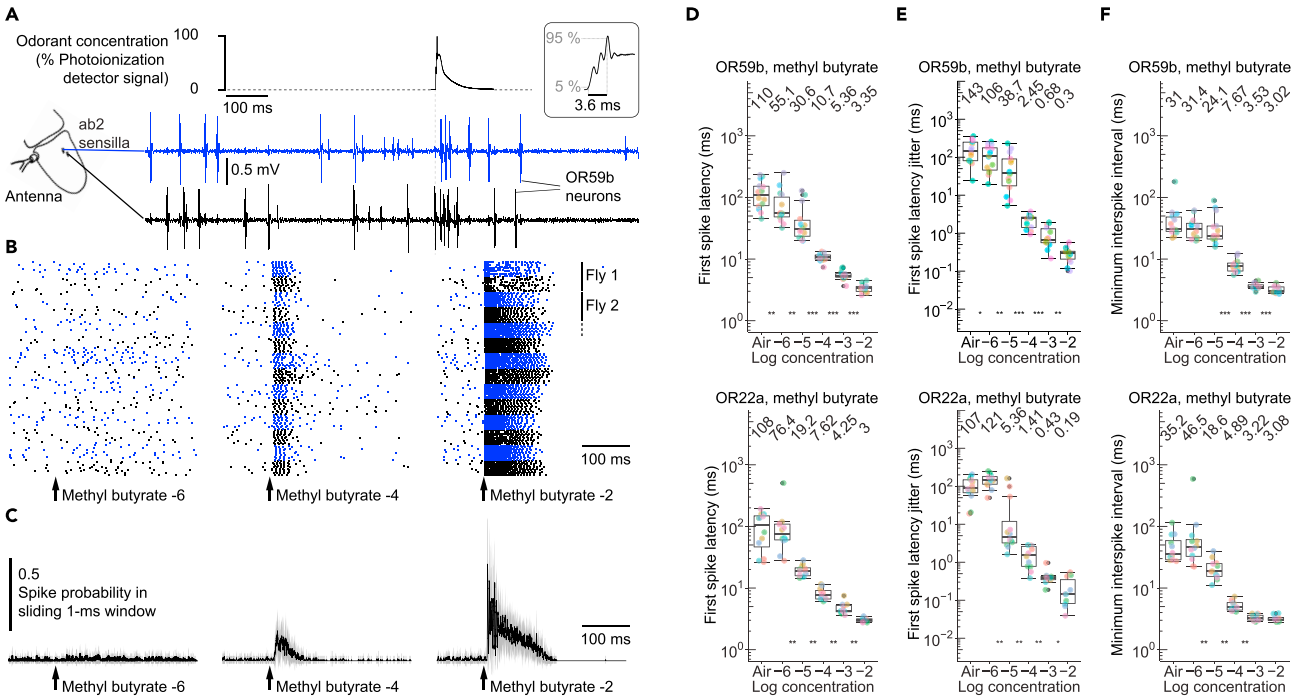

Figure 1. Timing of First Spikes in Olfactory Receptor Neurons Varies Over a Wider Concentration Range than Spike Rates

(A) Simultaneous, extracellular recordings from two OR59b neurons in two different ab2 sensilla during a pulse of methyl butyrate at a concentration of 10^{-4}. Top: Odorant stimulus measured with a photoionization detector. Timescale bar refers to both panels. Inset: Odorant onset (3.6 ms rise time, mean ± SD over ten stimulus repetitions).

(B) Raster plot of spikes in seven simultaneously recorded pairs of OR59b neurons during stimulation with methyl butyrate at different concentrations (10^{-6}, 10^{-4}, 10^{-2}).

(C) Same data as in (B) presented as spike probability in a sliding 1 ms window (mean ± SD over 14 OR59b neurons).

(D–F) First spike latencies (D), trial-to-trial jitter of first spike latencies (E), and minimum interspike intervals (1/maximum spike rate) (F) for OR59b and OR22a neurons during stimulation with different concentrations of methyl butyrate. Boxplots show the median and interquartile range across 14 OR59b and 12 OR22a neurons (same colored points represent same neuron). Numbers at the top indicate the median.

Stars indicate significant difference between medians of neighboring concentrations (*p < 0.05, **p < 0.01, ***p < 0.001). See also Figures S1 and S2.

et al., 2014; van Breugel and Dickinson, 2014), we presented brief odorant pulses with rapid changes in concentration (Figure 1A).

First Spike Timing Varies Over a Wider Concentration Range than Spike Rate

Odorant-evoked spikes were tightly locked to the onset of odorant pulses (Figures 1B, 1C, S1B, and S1C), with first spike latencies ranging from 18 to 55 ms for low concentrations and 3 to 4.4 ms for high concentrations (median latencies for 10 repeated stimulations; Figures 1D and S2A). First spike latencies were temporally precise across trials, with an average SD (trial-to-trial jitter) of 4.36–106 ms for low odorant concentrations and 0.19–0.49 ms for high concentrations (Figures 1E and S2B). The neuron-to-neuron jitter was similar to the trial-to-trial jitter and ranged from 4.82 to 107 ms for low concentrations and 0.2–0.91 ms for high concentrations (Figure S2C). First spike latency, jitter, and spike rate varied with odorant concentration, and first spike latencies varied over a wider concentration range than spike rates (represented as minimum interspike or first-to-second spike interval; Figures 1D–1F and S2).

The concentration dependency of response latencies has been previously reported in insects (Martelli et al., 2013) and vertebrates (Duchamp-Viret et al., 1999; Getchell and Shepherd, 1978). However, the minimum odorant-evoked first spike latency of 3 ms that we found (Figures 1 and S2A) is shorter than previously reported for insect olfactory receptor neurons (10–30 ms [De Bruyne et al., 2001; Schneider et al., 1964]) or vertebrate olfactory receptor neurons (50 ms [Firestein et al., 1990]). Likewise, the minimum first spike latency jitter of 0.19 ms (Figures 1 and S2B) is more than one order of magnitude smaller than previously reported for insect olfactory receptor neurons (7 ms jitter [Jeanne and Wilson, 2015]) or for vertebrate

olfactory receptor neurons (12 ms jitter [Shusterman et al., 2011]). Such a high spike timing precision is comparable with the precision of insect photoreceptor cells (0.1 ms jitter [Tatler et al., 2000]) or insect auditory receptor cells (0.16 ms jitter [Rokem et al., 2005]).

Our finding of shorter response latencies and higher spike timing precision than in previous studies could be explained by the short stimulus rise time (5% to 95% within 3.6 ms) of our olfactory stimulator, which is one to two orders of magnitude shorter than the stimulus rise time of commonly used olfactory stimulators (Martelli et al., 2013; Raiser et al., 2016), and by the fact that response strength and precision of insect olfactory receptor neurons increase with decreasing stimulus rise time (Kim et al., 2011; Martelli et al., 2013; Nagel and Wilson, 2011; Tichy et al., 2005, 2016).

Anatomical Convergence Allows Rapid Odorant Onset Detection

The detection of an odorant requires separating odorant-evoked from spontaneous spikes. We quantified this separation as detection accuracy (d_a), which is the difference between the mean number of odorant-evoked and spontaneous spikes divided by their root-mean-square SD (Jeanne and Wilson, 2015; Simpson and Fitter, 1973) (Figure 2A and Transparent Methods). We calculated the detection accuracy for a pool of 23 OR59b and of 8 OR22a neurons, because in female flies, about 23 OR59b and 8 OR22a neurons coalesce in different glomeruli (DM4 and DM2) of the antennal lobe (Grabe et al., 2016) and because all receptor neurons converge onto all uniglomerular projection neurons (Kazama and Wilson, 2009). Detection accuracy increased with the spike integration time window (integration time) (Figures 2B and S3) and with the number of receptor neurons (Figures 2C and S4). For a given odorant concentration, detection accuracy first increased independently of integration time (first 1 to 2 ms) and continued increasing with longer integration times (Figures 2B and S3A).

To estimate how odorant detection speed depends on concentration, we determined the minimum integration time to reach a threshold detection accuracy above five (Figure 2A), which corresponds to a false-positive rate of less than 1% for separating odorant-evoked from spontaneous spikes (see Transparent Methods). This detection accuracy threshold was reached with integration times between 10 and 16 ms already at the lowest odorant concentrations, and with integration times of less than 3 ms at intermediate concentrations. Importantly, at all concentrations this detection accuracy threshold was reached with an integration time that is shorter than the corresponding minimum interspike interval (1/spike rate) (Figures 2D, 1F, and S2). This indicates that the first odorant-evoked spikes across a population of 23 OR59b or 8 OR22a neurons are sufficient for encoding the onset of an odorant, even at low odorant concentrations.

Encoding of Odorant Identity with Spike Latencies

First spike latencies (relative to odorant arrival at the antenna) were temporally precise and odorant-specific (Figures 1D and S2A). Could the olfactory system use first spike latencies to encode odorant identity? First spike latencies may seem unsuitable for encoding odors, because the decoder does not know when the stimulus started. However, the olfactory system could use the difference of first spike latencies across different receptor neuron types (relative spike latencies), as has been demonstrated for other sensory systems (Gollisch and Meister, 2008; Thomson and Kristan, 2006; Thorpe et al., 2001). To test whether relative spike latencies across receptor neuron types could encode odorant identity, we compared the across-neuron pattern of first spike latencies and spike rates (minimum interspike intervals) (Figures 3A and 3B). OR59b neurons responded faster (shorter first spike latencies) and with higher spike rates (shorter inter spike intervals) to ethyl acetate than OR22a neurons, whereas OR22a neurons responded slightly faster and with higher spike rates to methyl butyrate than OR59b neurons. Both the difference in first spike latencies and the difference in interspike intervals (1/rate) between the two receptor neuron types allowed concentration-invariant classification of odorant identity across four to five orders of magnitude in concentration using a single classification threshold for all concentrations (0.76 ms difference in first spike latencies and 0.77 ms difference in interspike intervals) (Figure 3C and see Audios S1, S2, S3, S4, S5, S6, S7, S8, S9, S10, and S11 for audible examples of odorant-evoked spikes across 23 OR59b and 8 OR22a neurons).

Based on these results, we propose a coding scheme in which the first wave of odorant-evoked spikes across the population of the first responding olfactory receptor neuron type encodes the onset of an odorant (spikes are almost in synchrony, due to low jitter, Figures 1C and 1E), whereas the rank order (relative spike latencies, Figures 3A and 3C) of the subsequently responding olfactory receptor neuron types encodes the identity of that odorant in a concentration-invariant manner. Rank order codes for odorant

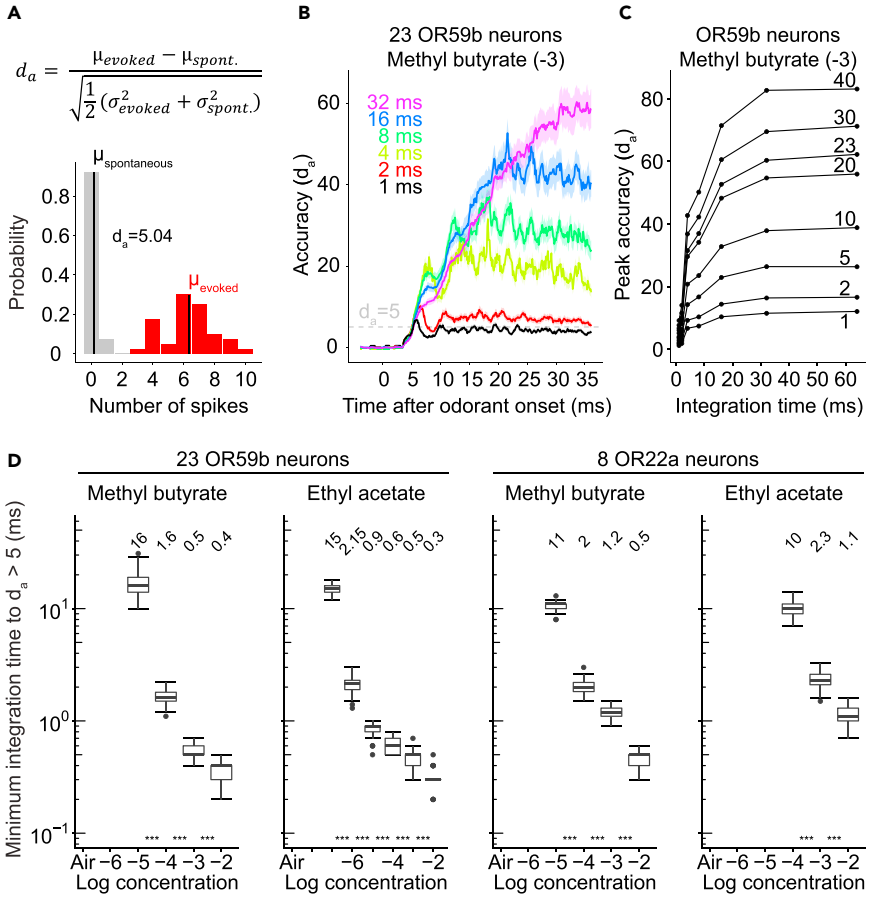

Figure 2. Anatomical Convergence Allows Rapid Odorant Onset Detection

(A) Odorant detection accuracy (d_a) was measured as the difference between the means of odorant-evoked (red) and spontaneous spike counts (gray), normalized to the SD of both. Distributions of spontaneously generated spikes and odorant-evoked spikes of a pool of 23 OR59b neurons (methyl butyrate at a concentration of 10^{-3}, integration time [1 ms], μ = mean, σ = SD).

(B) Detection accuracy (d_a, mean ± SD) computed for randomly selected pools of 23 OR59b neurons for different integration times (1–32 ms) during stimulation with methyl butyrate at a concentration of 10^{-3}.

(C) Peak detection accuracy (d_a) for different integration times (1, 2, 4, 8, 16, 32, 64 ms) and OR59b neuron pool sizes (1–40).

(D) Minimum integration time to exceed a detection accuracy of five during stimulation with different concentrations of methyl butyrate or ethyl acetate. Boxplots show the median and interquartile range for 50 repetitions, each computed from 40 random combinations of 23 OR59b or 8 OR22a neurons. At missing entries, the detection accuracy did not exceed five within an integration time window of 40 ms. Numbers at the top indicate the median. Stars indicate statistical difference between medians of neighboring concentrations (***$p < 0.001$).

See also Figures S3 and S4.

identity have been previously proposed for insects (Brill et al., 2013; Krofczik et al., 2009; Martelli et al., 2013) and vertebrates (Junek et al., 2010; Schaefer and Margrie, 2012; Spors, 2006), although at slower timescales.

To test whether the insect olfactory system could use the millisecond short differences in spike latencies across olfactory receptor neurons for odor coding, we built a spiking neural network for odorant classification, which contains network motifs of the second layer of olfactory processing, the mushroom body (Figure 3D). All neurons were simulated with a leaky integrate-and-fire model, using the same approach as Jeanne and Wilson (Jeanne and Wilson, 2015). As input to the model we randomly selected 8 OR22a and 23 OR59b neurons from the pool of our recordings. OR22a and OR59b neurons converge onto different projection neurons (PN_X and PN_Y) (Grabe et al., 2016; Kazama and Wilson, 2009), which form

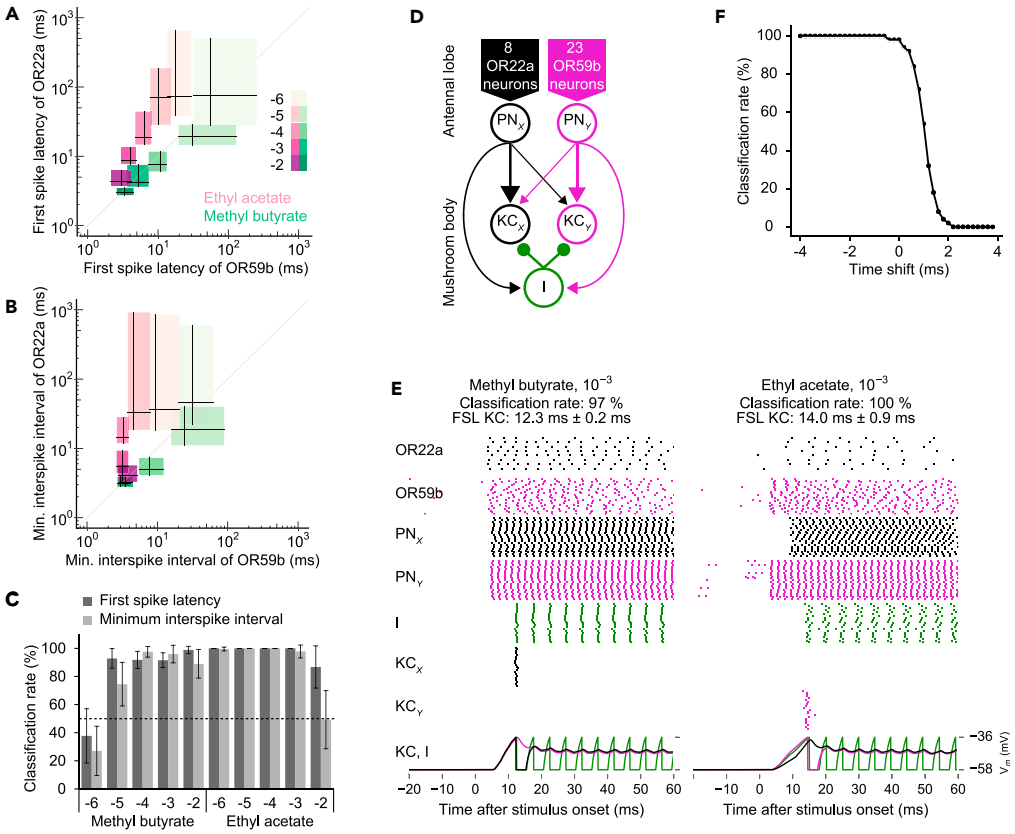

Figure 3. Relative Spike Latencies Allow Concentration-Invariant Rank Order Encoding of Odorant Identity

(A) First spike latencies of OR59b versus OR22a neurons for different concentrations of methyl butyrate and ethyl acetate (lines, median; boxes, 5th to 95th percentile range).

(B) Same as in (A) but for minimum interspike intervals.

(C) Classification of odorants based on the differences in first spike latencies or minimum interspike intervals between OR22a and OR59b neurons (mean ± SD). A single classification threshold was used across odorants and concentrations. Dashed line shows 50% chance level.

(D) Simplified spiking neural network model that is sensitive to the relative first spike latencies across receptor neuron types. Eight OR22a neurons form excitatory synapses with projection neuron PN_X and 23 OR59b neurons with PN_Y. PNs form excitatory synapses with two Kenyon cells (KC_X and KC_Y) and with an inhibitory neuron (I), which provides feedforward inhibition to both KCs. Individual PN-KC synapses differ in weight (arrow thickness reflects synaptic weights of PN-KC and PN-I synapses).

(E) Simulation results. From top to bottom: Recorded spikes in 8 OR22a and 23 OR59b neurons, simulated spikes in PN_X and PN_Y, I, KC_X and KC_Y, and simulated membrane potentials in I (green), KC_X (black), and KC_Y (magenta). Receptor neuron spike raster plots and membrane potentials show the first simulation, all other spike raster result from the first 20 simulations. Classification rate is the percentage of correct classifications during 100 simulation runs for each odorant. Odorant classification was correct when methyl butyrate induced a spike in KC_X but not in KC_Y and when ethyl acetate induced a spike in KC_Y but not in KC_X. Left: Methyl butyrate (concentration 10^{-3}) first activates OR22a and then OR59b neurons. Since the weight of the PN_X-KC_X synapse is larger than the weight of the PN_X-KC_Y synapse, the PN_X-driven inhibition prevents KC_Y from reaching its spiking threshold. Right: Ethyl acetate first activates OR59b and then OR22a and induces spikes in KC_Y but not in KC_X. FSL KC, first spike latency of Kenyon cells.

(F) To test the sensitivity of the network to the relative timing of spikes, the recorded spike trains (during stimulation with methyl butyrate, 10^{-3}) of all 8 OR22a neurons were shifted in time (from −4 to 4 ms relative to their original occurrence) in 0.2 ms steps while keeping the 23 OR59b spike trains unchanged. Classification rate (classified as methyl butyrate) decreases when spikes from OR22a neurons are shifted by 1–2 ms.

See also Figure S5 and Audios S1, S2, S3, S4, S5, S6, S7, S8, S9, S10, and S11.

excitatory synapses with different weights onto mushroom body intrinsic Kenyon cells (KC_X and KC_Y) (Gruntman and Turner, 2013). In addition, projection neurons provide feedforward inhibition onto Kenyon cells via an inhibitory neuron (I). Such an inhibitory feedforward circuit via a GABAergic neuron exists in

honey bees within the mushroom input region (calyx) (Ganeshina and Menzel, 2001), and it might also exist within the mushroom body calyx of other insects (e.g., *Drosophila* [Lei et al., 2013; Lin et al., 2014], locusts [Leitch and Laurent, 1996; Papadopoulou et al., 2011]). Note that for the sake of simplicity and as a proof of principle, we ignored several properties of the *Drosophila* olfactory systems (see Transparent Methods).

This network resembles a network model by Thorpe and colleagues (Thorpe et al., 2001), which is sensitive to the rank order of spike arrival times from different inputs, and it resembles a (recently refuted) model by Assisi and colleagues (Assisi et al., 2007; Gupta and Stopfer, 2012) in which Kenyon cells' integration time is shortened through feedforward inhibition. Notably, a similar circuit motif for the required rapid feedforward inhibition (Thorpe et al., 2001) also exists in the second layer of the vertebrate olfactory system, the olfactory cortex (Stokes and Isaacson, 2010). In our model, the depolarization of Kenyon cells depends on the different synaptic weights from projection neurons and is strongest when projection neurons are activated in the order of their synaptic weights (Figures 3E and S5). This is because feedforward inhibition increases with the number of inputs (see Thorpe et al. (2001) for a detailed analysis of a similar rank-order-sensitive network). Note that since inputs from PN_Y are weighted lower than inputs from PN_X, KC_X can respond even when PN_Y responds shortly before PN_X.

Using this rank-order-sensitive network, classification of the two odorants, based on the experimentally measured spike trains in OR22a and OR59b neurons, was rapid (within 10 and 28 ms after odorant arrival) and reliable (between 78% and 100% correct classification) at concentrations between 10^{-4} and 10^{-2} (Figures 3E and S5). To test the rank-order sensitivity of the model independently of spike rate differences, we repeated the simulations with artificially introduced time shifts in the experimentally measured spike trains of one olfactory receptor neuron type while leaving the other at its original time (Figure 3F). Odorant classification was correct, when the rank order was retained by the time shift, showing that the model is sensitive for the rank order of olfactory receptor neuron inputs. The exact time shift at which the classification decreases depends on the synaptic weights between the PN and KC, as stronger weights lead to a faster response in the respective KC. This simplified network model of the mushroom body demonstrates that odorant-specific response latencies across olfactory receptor neuron types, together with rapid feedforward inhibition, allow encoding of odorant identity with relative spike latencies.

Rapid odorant detection is likely not unique to *Drosophila* receptor neurons, as rapid odorant-evoked antennal responses occur in other insects (Szyszka et al., 2014), all of which face the challenge of detecting odorants when moving through turbulent air (Celani et al., 2014; Murlis, 1992). The need for speed could have promoted the evolution of pore tubules that accelerate odorant diffusion toward olfactory receptors (Maitani et al., 2010; Steinbrecht, 1997) and of rapid ligand-gated ionotropic olfactory receptors (Getahun et al., 2012; Sato et al., 2008; Silbering and Benton, 2010; Wicher et al., 2008) that allow faster stimulus transduction than metabotropic receptors (house fly photoreceptors, which are the fastest known metabotropic receptors, have a minimum response latency of 12 ms [Howard et al., 1984]).

Insect olfaction is similar to vertebrate audition in that both senses continuously sample the temporal structure of stimuli. The vertebrate auditory system relies on precise spike timing when it uses stimulus onset asynchrony and interaural time differences to separate and to localize sound sources (Knudsen and Konishi, 1979; Rasch, 1978). Analogous to the vertebrate auditory system, the insect olfactory system can use millisecond short stimulus onset asynchrony for odor source separation (Baker et al., 1998; Szyszka et al., 2012), and it may use bilateral time differences for source localization during active sampling of odorant gradients (Borst and Heisenberg, 1982; Duistermars et al., 2009; Gaudry et al., 2013; Hangartner, 1967; Louis et al., 2008). In addition to supporting odor source separation and localization, the high temporal precision of odor-evoked spikes across olfactory receptor neurons could allow the insect olfactory system to use a rapid, spike timing-based code for odorant identity.

METHODS

All methods can be found in the accompanying Transparent Methods supplemental file.

SUPPLEMENTAL INFORMATION

Supplemental Information includes Transparent Methods, 5 figures, 1 table, 11 audios, and 1 data file and can be found with this article online at https://doi.org/10.1016/j.isci.2018.05.009.

ACKNOWLEDGMENTS

We thank Stefanie Neupert and Aarti Sehdev for help with the data analysis and Giovanni Galizia, Thomas Nowotny, and Ho Ka Chan for comments on the manuscript. This work was funded by the Human Frontier Science Program (RGP0053/2015 to PS).

AUTHOR CONTRIBUTIONS

Conceptualization, A.R. and P.S.; Methodology, A.R., A.E.-W., and P.S.; Formal Analysis, A.R. and A.E.-W.; Investigation, A.R. and A.E.-W.; Resources, C.J.K. and P.S.; Writing – Original Draft, A.E.-W. and P.S.; Writing – Review & Editing, C.J.K, A.E.-W. and A.R., P.S.; Visualization, A.R., A.E.-W., and P.S.; Supervision, P.S.; Project Administration, P.S.; Funding Acquisition, P.S.

DECLARATION OF INTERESTS

The authors declare no competing interests.

Received: March 7, 2018
Revised: April 19, 2018
Accepted: May 14, 2018
Published: June 29, 2018

REFERENCES

Assisi, C., Stopfer, M., Laurent, G., and Bazhenov, M. (2007). Adaptive regulation of sparseness by feedforward inhibition. Nat. Neurosci. *10*, 1176–1184.

Baker, T.C., Fadamiro, H.Y., and Cosse, A.A. (1998). Moth uses fine tuning for odour resolution. Nature *393*, 530.

Borst, A., and Heisenberg, M. (1982). Osmotropotaxis in *Drosophila melanogaster*. J. Comp. Physiol. A *147*, 479–484.

van Breugel, F., and Dickinson, M.H. (2014). Plume-tracking behavior of flying *Drosophila* emerges from a set of distinct sensory-motor reflexes. Curr. Biol. *24*, 274–286.

Brill, M.F., Rosenbaum, T., Reus, I., Kleineidam, C.J., Nawrot, M.P., and Rossler, W. (2013). Parallel processing via a dual olfactory pathway in the honeybee. J. Neurosci. *33*, 2443–2456.

de Bruyne, M., Clyne, P.J., and Carlson, J.R. (1999). Odor coding in a model olfactory organ: the *Drosophila* maxillary palp. J. Neurosci. *19*, 4520–4532.

De Bruyne, M., Foster, K., and Carlson, J.R. (2001). Odor coding in the *Drosophila* antenna. Neuron *30*, 537–552.

Carr, C.E., and Konishi, M. (1990). A circuit for detection of interaural time differences in the brain stem of the barn owl. J. Neurosci. *10*, 3227–3246.

Celani, A., Villermaux, E., and Vergassola, M. (2014). Odor landscapes in turbulent environments. Phys. Rev. X *4*, 1–17.

Duchamp-Viret, P., Chaput, M.A., and Duchamp, A. (1999). Odor response properties of rat olfactory receptor neurons. Science *284*, 2171–2174.

Duistermars, B.J., Chow, D.M., and Frye, M.A. (2009). Flies require bilateral sensory input to track odor gradients in flight. Curr. Biol. *19*, 1301–1307.

Farrell, J.A., Murlis, J., Long, X., Li, W., and Cardé, R.T. (2002). Filament-based atmospheric dispersion model to achieve short time-scale structure of odor plumes. Environ. Fluid Mech. *2*, 143–169.

Firestein, S., Shepherd, G.M., and Werblin, F.S. (1990). Time course of the membrane current underlying sensory transduction in salamander olfactory receptor neurones. J. Physiol. *430*, 135–158.

Ganeshina, O., and Menzel, R. (2001). GABA-immunoreactive neurons in the mushroom bodies of the honeybee: an electron microscopic study. J. Comp. Neurol. *437*, 335–349.

Gaudry, Q., Hong, E.J., Kain, J., de Bivort, B.L., Wilson, R.I., de Bivort, B.L., and Wilson, R.I. (2013). Asymmetric neurotransmitter release enables rapid odour lateralization in *Drosophila*. Nature *493*, 424–428.

Getahun, M.N., Wicher, D., Hansson, B.S., and Olsson, S.B. (2012). Temporal response dynamics of *Drosophila* olfactory sensory neurons depends on receptor type and response polarity. Front. Cell. Neurosci. *6*, 54.

Getchell, T.V., and Shepherd, G.M. (1978). Responses of olfactory receptor cells to step pulses of odour at different concentrations in the salamander. J. Physiol. *282*, 521–540.

Gollisch, T., and Meister, M. (2008). Rapid neural coding in the retina with relative spike latencies. Science *319*, 1108–1111.

Grabe, V., Baschwitz, A., Dweck, H.K.M., Lavista-Llanos, S., Hansson, B.S., and Sachse, S. (2016). Elucidating the neuronal architecture of olfactory glomeruli in the *Drosophila* antennal lobe. Cell Rep. *16*, 3401–3413.

Gruntman, E., and Turner, G.C. (2013). Integration of the olfactory code across dendritic claws of single mushroom body neurons. Nat. Neurosci. *16*, 1821–1829.

Gupta, N., and Stopfer, M. (2012). Functional analysis of a higher olfactory center, the lateral horn. J. Neurosci. *32*, 8138–8148.

Hangartner, W. (1967). Spezifität und Inaktivierung des Spurpheromons von Lasius fuliginosus Latr. und Orientierung der Arbeiterinnen im Duftfeld. Z. Vgl. Physiol. *57*, 103–136.

Howard, J., Dubs, A., and Payne, R. (1984). The dynamics of phototransduction in insects. J. Comp. Physiol. A *154*, 707–718.

Huston, S.J., Stopfer, M., Cassenaer, S., Aldworth, Z.N., and Laurent, G. (2015). Neural encoding of odors during active sampling and in turbulent plumes. Neuron *88*, 403–418.

Jeanne, J.M., and Wilson, R.I. (2015). Convergence, divergence, and reconvergence in a feedforward network improves neural speed and accuracy. Neuron *88*, 1014–1026.

Junek, S., Kludt, E., Wolf, F., and Schild, D. (2010). Olfactory coding with patterns of response latencies. Neuron *67*, 872–884.

Kazama, H., and Wilson, R.I. (2009). Origins of correlated activity in an olfactory circuit. Nat. Neurosci. *12*, 1136–1144.

Kim, A.J., Lazar, A.A., and Slutskiy, Y.B. (2011). System identification of *Drosophila* olfactory sensory neurons. J. Comput. Neurosci. *30*, 143–161.

Knudsen, E.I., and Konishi, M. (1979). Mechanisms of sound localization in the barn owl (Tyto alba). J. Comp. Physiol. A *133*, 13–21.

Krofczik, S., Menzel, R., and Nawrot, M.P. (2009). Rapid odor processing in the honeybee antennal lobe network. Front. Comput. Neurosci. *2*, 9.

Lei, Z., Chen, K., Li, H., Liu, H., and Guo, A. (2013). The GABA system regulates the sparse coding of odors in the mushroom bodies of *Drosophila*. Biochem. Biophys. Res. Commun. *436*, 35–40.

Leitch, B., and Laurent, G. (1996). GABAergic synapses in the antennal lobe and mushroom body of the locust olfactory system. J. Comp. Neurol. *372*, 487–514.

Lin, A.C., Bygrave, A.M., de Calignon, A., Lee, T., and Miesenböck, G. (2014). Sparse, decorrelated odor coding in the mushroom body enhances learned odor discrimination. Nat. Neurosci. *17*, 559–568.

Louis, M., Huber, T., Benton, R., Sakmar, T.P., and Vosshall, L.B. (2008). Bilateral olfactory sensory input enhances chemotaxis behavior. Nat. Neurosci. *11*, 187–199.

Maitani, M.M., Allara, D.L., Park, K.C., Lee, S.G., and Baker, T.C. (2010). Moth olfactory trichoid sensilla exhibit nanoscale-level heterogeneity in surface lipid properties. Arthropod. Struct. Dev. *39*, 1–16.

Martelli, C., Carlson, J.R., and Emonet, T. (2013). Intensity invariant dynamics and odor-specific latencies in olfactory receptor neuron response. J. Neurosci. *33*, 6285–6297.

Murlis, J. (1992). Odor plumes and how insects use them. Annu. Rev. Entomol. *37*, 505–532.

Nagel, K.I., and Wilson, R.I. (2011). Biophysical mechanisms underlying olfactory receptor neuron dynamics. Nat. Neurosci. *14*, 208–216.

Papadopoulou, M., Cassenaer, S., Nowotny, T., and Laurent, G. (2011). Normalization for sparse encoding of odors by a wide-field interneuron. Science *332*, 721–725.

Raiser, G., Galizia, C.G.G., and Szyszka, P. (2016). A high-bandwidth dual-channel olfactory stimulator for studying temporal sensitivity of olfactory processing. Chem. Senses *42*, 141–151.

Rasch, R. (1978). The perception of simultaneous notes such as in polyphonic music. Acta Acust. united Ac. *40*, 21–33.

Riffell, J.A., Shlizerman, E., Sanders, E., Abrell, L., Medina, B., Hinterwirth, A.J., and Kutz, J.N. (2014). Sensory biology. Flower discrimination by pollinators in a dynamic chemical environment. Science *344*, 1515–1518.

Rokem, A., Watzl, S., Gollisch, T., Stemmler, M., Herz, A.V.M., and Samengo, I. (2005). Spike-timing precision underlies the coding efficiency of auditory receptor neurons. J. Neurophysiol. *95*, 2541–2552.

Sato, K., Pellegrino, M., Nakagawa, T., Nakagawa, T., Vosshall, L.B., and Touhara, K. (2008). Insect olfactory receptors are heteromeric ligand-gated ion channels. Nature *452*, 1002–1006.

Schaefer, A.T., and Margrie, T.W. (2012). Psychophysical properties of odor processing can be quantitatively described by relative action potential latency patterns in mitral and tufted cells. Front. Syst. Neurosci. *6*, 30.

Schneider, D., Lacher, V., and Kaissling, K.E. (1964). Die Reaktionsweise und das Reaktionsspektrum von Riechzellen bei Antheraea pernyi (Lepidoptera, Saturniidae). Z. Vgl. Physiol. *48*, 632–662.

Shusterman, R., Smear, M.C., Koulakov, A.A., and Rinberg, D. (2011). Precise olfactory responses tile the sniff cycle. Nat. Neurosci. *14*, 1039–1044.

Silbering, A.F., and Benton, R. (2010). Ionotropic and metabotropic mechanisms in chemoreception: "chance or design"? EMBO Rep. *11*, 173–179.

Simpson, A.J., and Fitter, M.J. (1973). What is the best index of detectability? Psychol. Bull. *80*, 481–488.

Spors, H. (2006). Temporal dynamics and latency patterns of receptor neuron input to the olfactory bulb. J. Neurosci. *26*, 1247–1259.

Steinbrecht, R.A. (1997). Pore structures in insect olfactory sensilla: a review of data and concepts. Int. J. Insect Morphol. Embryol. *26*, 229–245.

Stokes, C.C.A., and Isaacson, J.S. (2010). From dendrite to soma: dynamic routing of inhibition by complementary interneuron microcircuits in olfactory cortex. Neuron *67*, 452–465.

Szyszka, P., Stierle, J.S.J.S., Biergans, S., and Galizia, C.G.G. (2012). The speed of smell: odor-object segregation within milliseconds. PLoS One *7*, e36096.

Szyszka, P., Gerkin, R.C., Galizia, C.G.G., and Smith, B.H.B.H. (2014). High-speed odor transduction and pulse tracking by insect olfactory receptor neurons. Proc. Natl. Acad. Sci. USA *111*, 16925–16930.

Tatler, B., O'Carroll, D.C., and Laughlin, S.B. (2000). Temperature and the temporal resolving power of fly photoreceptors. J. Comp. Physiol. A *186*, 399–407.

Thomson, E.E., and Kristan, W.B. (2006). Encoding and decoding touch location in the leech CNS. J. Neurosci. *26*, 8009–8016.

Thorpe, S., Delorme, A., and Van Rullen, R. (2001). Spike-based strategies for rapid processing. Neural Netw. *14*, 715–725.

Tichy, H., Hinterwirth, A., and Gingl, E. (2005). Olfactory receptors on the cockroach antenna signal odour ON and odour OFF by excitation. Eur. J. Neurosci. *22*, 3147–3160.

Tichy, H., Hellwig, M., and Zopf, L.M. (2016). The rate of concentration change and how it determines the resolving power of olfactory receptor neurons. Front. Physiol. *7*, 645.

Vickers, N. (2000). Mechanisms of animal navigation in odor plumes. Biol. Bull. *198*, 203–212.

Wicher, D., Schäfer, R., Bauernfeind, R., Stensmyr, M.C., Heller, R., Heinemann, S.H., and Hansson, B.S. (2008). *Drosophila* odorant receptors are both ligand-gated and cyclic-nucleotide-activated cation channels. Nature *452*, 1007–1011.

ISCI, Volume *4*

Supplemental Information

High Precision of Spike Timing across Olfactory Receptor Neurons Allows Rapid Odor Coding in *Drosophila*

Alexander Egea-Weiss, Alpha Renner, Christoph J. Kleineidam, and Paul Szyszka

Supplemental Figures

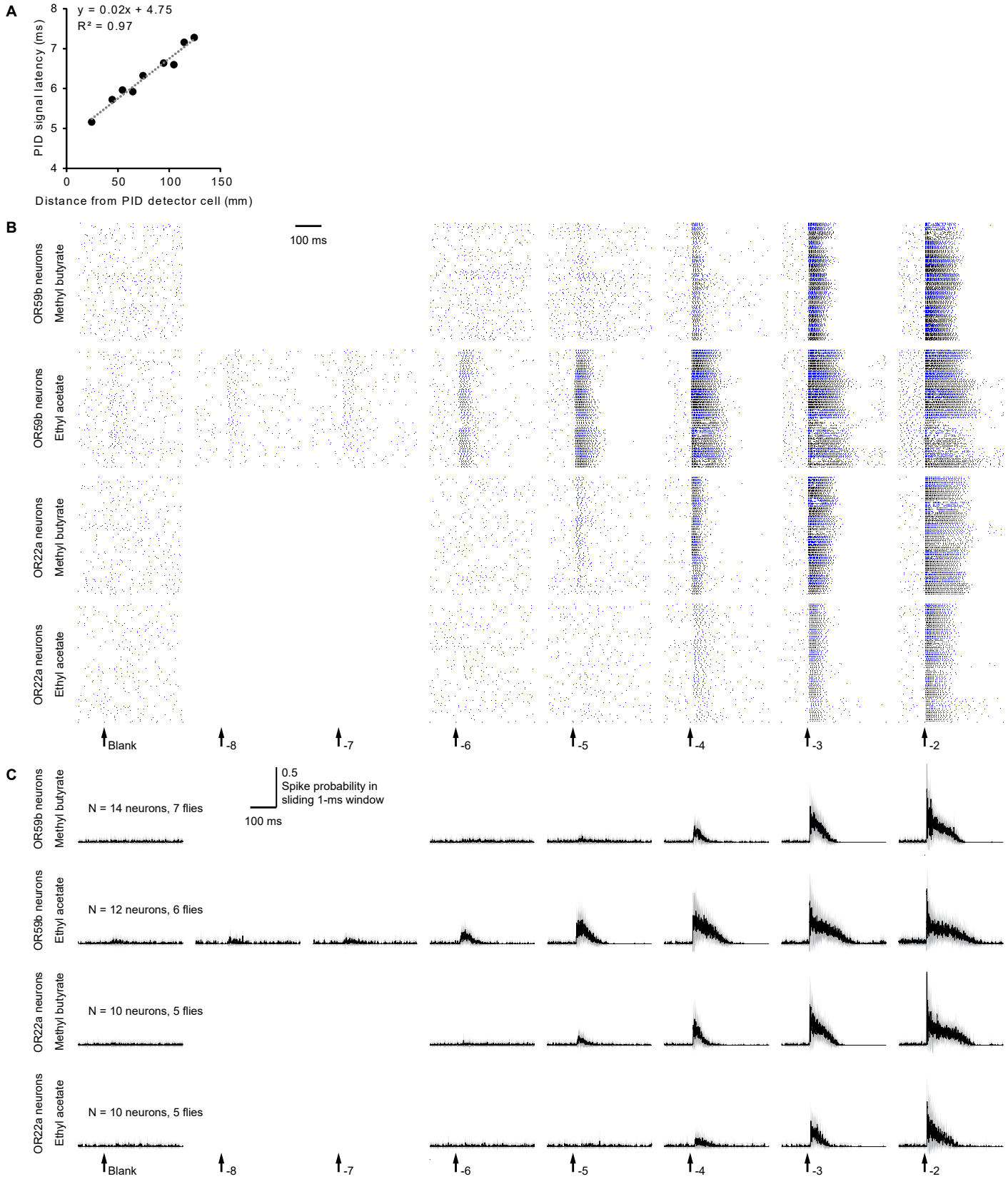

Figure S1. Reproducible, concentration-dependent spike responses across neurons and flies, Related to Figure 1 and Transparent Methods. (A) Stimulus latency was determined with a photoionization detector (PID, miniPID, Aurora) and ethyl acetate (10^{-2}) as tracer substance. A 125 mm long glass tube served as inlet of the PID. The glass tube ended at the detector cell. The length of the glass tube was gradually shortened, while measuring the PID signal latency. The PID signal latency decreased linearly ($R^2 = 0.97$, linear regression) with the decrease of the distance to the detector cell. The 4.75 ms stimulus latency was extrapolated as the time at which the distance to the detector cell was 0 mm (intercept with the y-axis). (B) Raster plot of simultaneously recorded spikes in pairs of OR59b and OR22a neurons during 10 blank or odorant stimuli (methyl butyrate or ethyl acetate) at different concentrations (10^{-8} to 10^{-2}). Adjacent blue and black points represent spikes from simultaneously recorded neuron pairs. (C) Same data as in (B) presented as spiking probability during sliding 1 ms windows (mean ± SD).

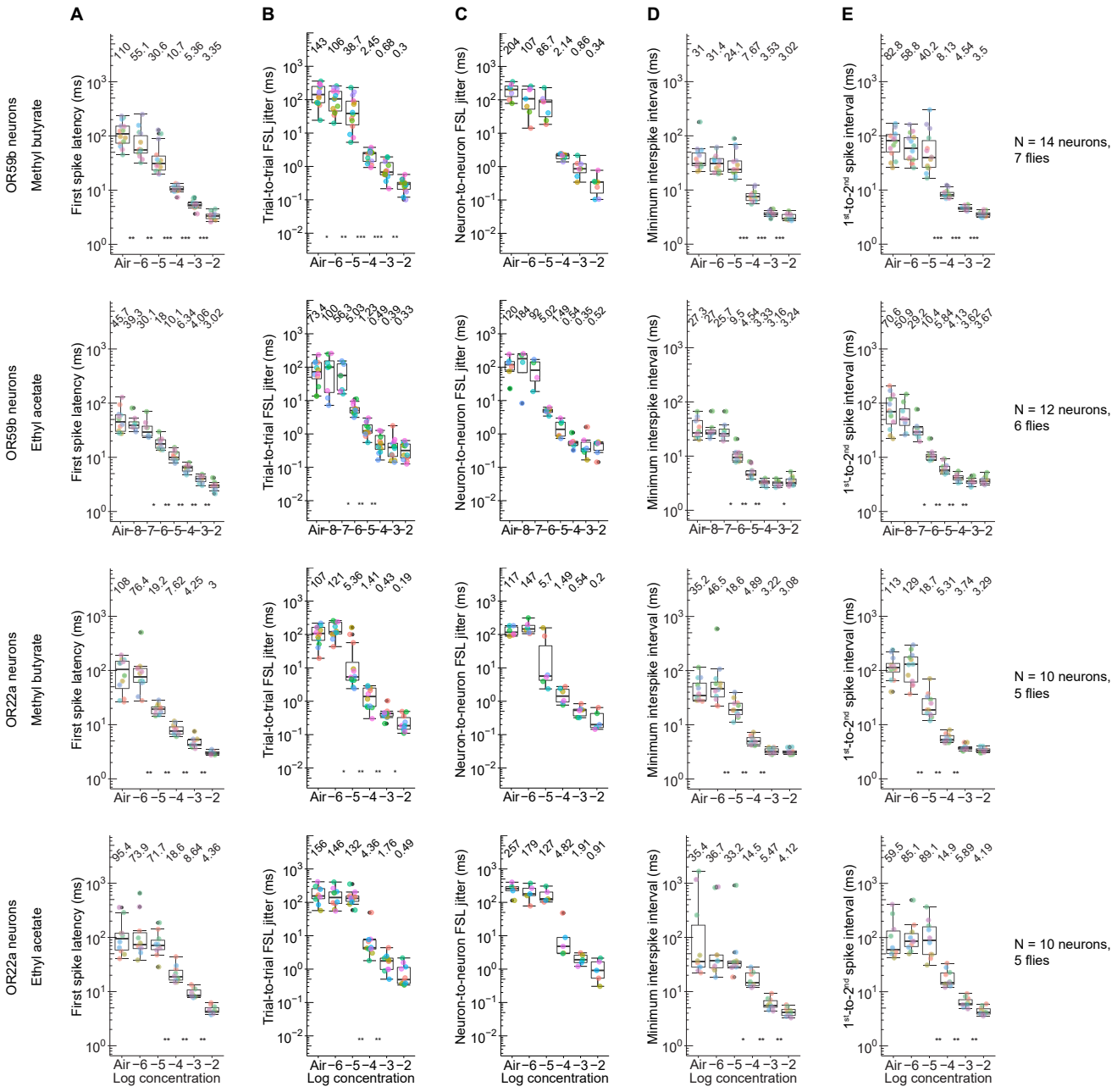

Figure S2. First spike timing varies over a wider concentration range than spike rate, Related to Figure 1.

(A – E) First spike latencies (A), trial-to-trial jitter of first spike latencies (FSL) (B), neuron-to-neuron jitter of first spike latencies (C), minimum interspike intervals (1/maximum rate) (D), and interval between the first and second spikes after odorant onset (E) for OR59b and OR22a neurons during stimulation with different concentrations of methyl butyrate or ethyl acetate. Boxplots show the median and interquartile range across neurons (colored points, same color represents same neuron). Numbers at the top indicate the median. Stars indicate statistical difference between medians of neighboring concentrations (* p<0.05, ** p<0.01, *** p<0.001).

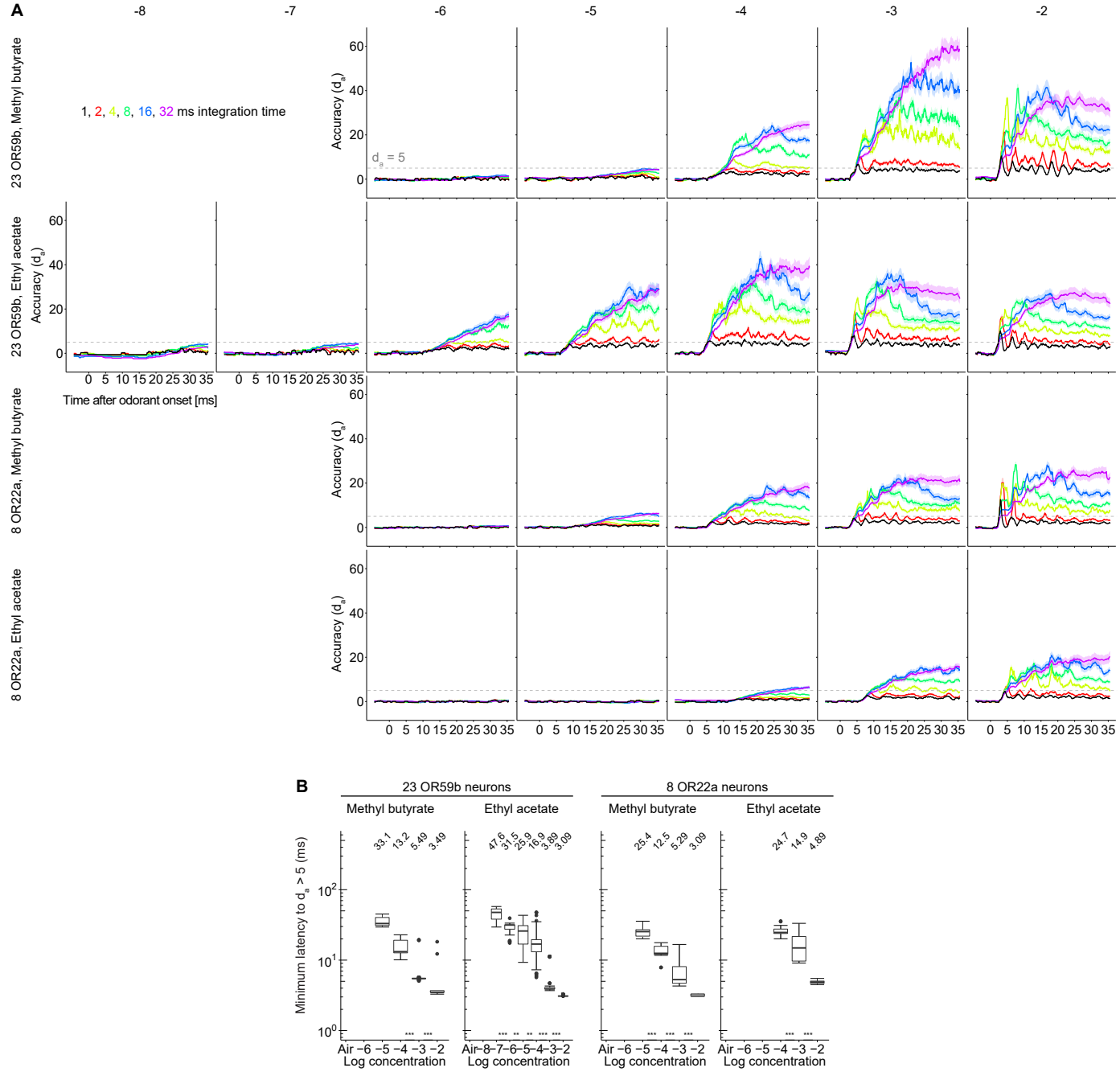

Figure S3. Stimulus detection accuracy depends on odorant concentration and integration time, Related to Figure 2.

(A) Stimulus detection accuracy (da, mean ± SD) computed for a simulated pool of 23 OR59b and 8 OR22a neurons for different integration time windows (1 – 32 ms) during stimulation with methyl butyrate and ethyl acetate at different concentrations (10^{-8} – 10^{-2}).(B) Minimum latency (first spike latency + same integration time windows as in Figure 2D) to reach a detection accuracy above 5 during stimulation with different concentrations of methyl butyrate and ethyl acetate in 23 OR59b and 8 OR22a neurons. At missing entries the detection accuracy did not exceed 5 within an integration time window of 40 ms. Numbers at the top indicate the median. Stars indicate statistical difference between medians of neighboring concentrations (** p<0.01, *** p<0.001).

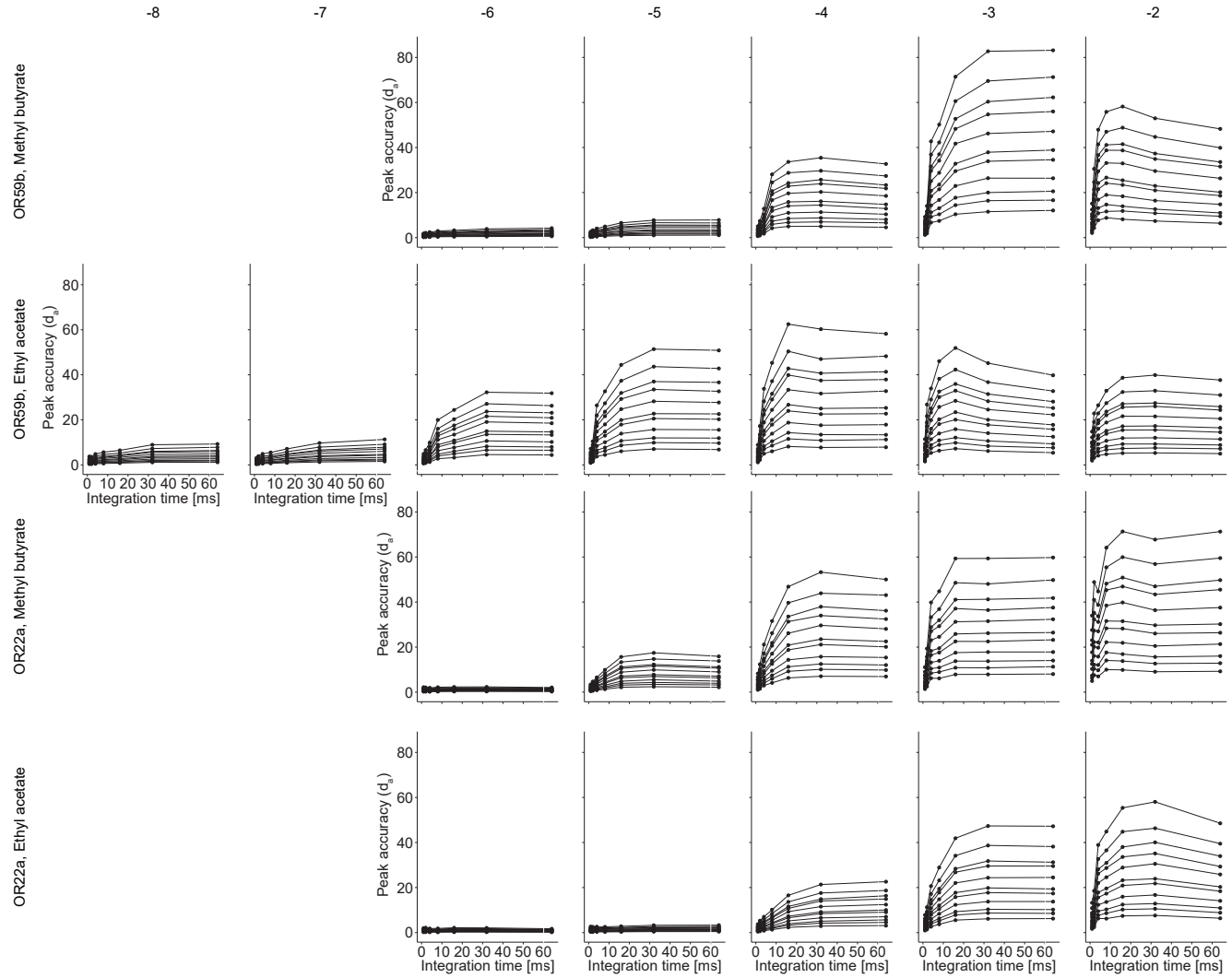

Figure S4. Peak detection accuracy depends on odorant concentration, neuron number and integration time window, Related to Figure 2.
Peak stimulus detection accuracy (da) for different integration time windows (1 – 64 ms) and number of neurons (1, 2, 3, 5, 8, 10, 15, 20, 23, 30, 40) for stimulation with methyl butyrate and ethyl acetate at different concentrations (10^{-8} – 10^{-2}).

Figure S5. Simulation results from the spiking neural network model for odorant classification, Related to Figure 3.

In each panel, from top to bottom: Recorded spikes in 8 OR22a and 23 OR59b neurons, simulated spikes in PNX and PNY, I, KCX and KCY, and simulated membrane potentials in I (green), KC_X (black) and KC_Y (magenta). Left: Methyl butyrate (concentration 10^{-3}) first activates OR22a neurons and then OR59b neurons. Right: Ethyl acetate first activates OR59b neurons and then OR22a neurons and induces spikes in KC_Y but not in KC_X. Odorant classification was correct when methyl butyrate induced a spike response in KC_X but not in KC_Y and when ethyl acetate induced a spike response in KC_Y but not in KC_X. Classification rate was calculated as the percentage of correct classifications during 100 simulation runs for each odorant. Receptor neuron spike raster and membrane potentials result from the first simulation, all other spike raster result from the first 20 simulations. Note that in this model classification only works reliably for higher concentrations, because in order to be activated, each KC requires inputs from both PNs in the right order.

Supplemental Table

Table S1. Parameters of model neurons, Related to Figure 3. Parameters of PNs and PN-ORN synapses are the same or close to the ones from (Jeanne and Wilson, 2015; Nagel and Wilson, 2011). Parameters of KCs and PN-KC synapses are the same or close to the ones from (Turner et al., 2008). In (Turner et al., 2008) values were given per unit, which explains the large difference to the PN parameters. Note that for the simulation only relative values within a neuron and its pre-synapses matter. For the inhibitory neuron (I) we took the same parameters as for KC, due to a lack of published data. Free parameters that were tuned to achieve a good classification rate were the synaptic weights (J) PN-KC, PN-I and I-KC.

Neuron parameter	**PN**	**KC, I**
G_l (leak conductance)	4.35 nS	90 µS
V_{res} (reset and leak reversal potential)	-55 mV	-58 mV
V_{thr} (threshold potential)	-40 mV	-36 mV
C_m (membrane capacitance)	0.135 pF	1µF
t_{ref} (refractory period)	2 ms	3 ms

Synapse parameter	**ORN-PN**	**PN-KC, PN-I**	**I-KC**
τ (EPSG time scale)	3 ms	3 ms	3 ms
V_{rev} (reversal potential)	0 mV	0 mV	-65 mV
J (EPSG peak amplitude)	0.27 nS	J_{XX} = 70 µS	400 µS
		$J_{YY} = 0.81 * J_{XX}$	
		$J_{XY} = 0.5 * J_{XX}$	
		$J_{YX} = 0.5 * J_{YY}$	
		$J_{PN-I} = (J_{XX} + J_{YY} + J_{XY} + J_{YX})/4$	

Transparent Methods

Fly stock and maintenance

All experiments were done with 2 – 7 days old, female wild-type Canton-S *Drosophila melanogaster*. Flies were raised at 25 °C on standard *Drosophila* medium, with a 12/12 h day/night cycle.

Fly preparation

Electrophysiological recordings of olfactory receptor neurons were performed on large basiconic ab2 sensilla (OR59b neurons) and ab3 sensilla (OR22a neurons) of the left antenna. The fly was fixed in a 200 µL plastic pipette tip with a piece of cotton, and the left antenna was glued with low melting wax (1:1:1 mixture of n-eicosan, myristic acid and dental wax (Deiberit 502; Dr. Böhme und Schöps Dental)) to gain access to the medial side. The right antenna was covered with low melting wax. The two recording electrodes were positioned with micromanipulators (Kleindieck) and inserted into two sensilla of the same type under a microscope (Axioplan, Zeiss) equipped with a 50x objective (LMPlanFl 50x/0.50, Olympus). The identity of the large basiconic ab2 and ab3 sensilla was determined by their response to a panel of 5 diagnostic odorants (methyl butyrate, isobutyl acetate, methyl acetate, 2-butanone and ethyl hexanoate at a concentration of 10^{-3}, all from Sigma Aldrich) which were applied as 500 ms long pulses via a multichannel odorant delivery device (Szyszka et al., 2011). Deflections in the sensillum potential and increase in spike rate were taken as excitatory responses to a given odorant. Sensilla showing moderate responses to 2-butanone and strong responses to methyl butyrate and methyl acetate were identified as ab2 sensilla, whereas sensilla responding strongly to methyl butyrate, isobutyl acetate and ethyl hexanoate were identified as ab3 sensilla (Database of Odorant Responses, (Münch and Galizia, 2016)).

Electrophysiology

Tungsten wires (diameter = 0.1mm) that were electrolytically sharpened with AC-current in a 0.5 M KOH solution were used as recording and reference electrodes. Two recording electrodes were inserted in two sensilla of the same type, and the reference electrode was inserted into the complex eye. Lubricant gel (Hydro Sensitiv Gel, Ritex) was applied to the contact zone between the reference electrode and the eye in order to increase electric conductance and to keep the eye from drying out. Signals of the recording electrodes were differentially amplified against the reference electrode using 1000x gain and a 1.0 Hz and 8.0 kHz bandpass filter (MA 103 preamplifier and MA 102 4-channel amplifier, Universität zu Köln). Noise from the powerline was reduced with a Hum Bug (Quest Scientific) and signals were digitized with a Micro 3 1401 (CED). Stimulation and recordings were controlled with Spike2 software (version 7.03 CED).

Odorant delivery

Methyl butyrate and ethyl acetate (Sigma-Aldrich) were diluted in 10 mL mineral oil (Sigma-Aldrich) in 120-mL headspace bottles. During experiments, the odorant solutions were continuously stirred with a magnetic stirrer to create an equilibrated headspace. Odorant solutions were freshly made every month (corresponds to approximately 10 stimulations). Fast odorant pulses were applied by opening a 3-way solenoid valve for 3 ms (LFAA1200118H; Lee) (Szyszka et al., 2014). The flow rate was adjusted to 190 mL per minute (charcoal-filtered air, non-humidified, digital air pressure control (35898; Analyt-MTC) and flow control (rotameter, 112-02GL; Analyt-MTC)). The inner diameter of the Teflon tube at the stimulator outlet was 1 mm, the distance between the stimulator outlet and the antenna was 1 mm, and the distance between antenna and the gate of the valve was 16.5 mm. The gate of the valve starts moving around 0.4 ms after the electrical trigger signal that switches the valve (Szyszka et al., 2014). Assuming a laminar airflow and no pressure changes, the odorant would arrive 4.5 ms after the trigger signal that operated the valve (0.4-ms valve delay plus 4.1-ms air travel time).

We determined the actual stimulus latency (time between the valve trigger and the arrival of the odorant at the antenna) with a photoionization detector (PID, miniPID, Aurora), using ethyl acetate (10^{-2}) as tracer substance. The inlet needle of the PID was replaced by a 125 mm long glass tube that ended at the PID detector cell, and the PID pump was set to the highest speed. The length of the glass tube was gradually shortened, while measuring the PID signal latency for ten stimulus repetitions. The PID signal latency was determined by first averaging the PID signal over the ten stimulus repetitions in order to decrease noise, and then moving backwards from the time where the response is 5 standard deviations above baseline until the PID signal reached the baseline (mean PID signal over first 4 ms after valve trigger). The PID signal latency decreased linearly ($R^2 = 0.97$, linear regression) with decreasing

distance to the PID detection cell (Figure S1A). The stimulus latency of 4.75 ms was extrapolated, and corresponds to the time at which the distance to the detection cell would be 0 mm. This value was subtracted from all spike latencies.

This olfactory stimulator generates fast changes in odorant concentration (rise time 5%-to-95% within 3.6 ms, Figure 1A), and is one to two orders of magnitude faster than commonly used olfactory stimulators (Martelli et al., 2013). We delivered sequences of 10 odorant pulses by opening the valve for 3 ms, with an interpulse interval of 5 s. We applied series of odorant pulses with different concentrations (10^{-8}, 10^{-7}, 10^{-6}, 10^{-5}, 10^{-4}, 10^{-3}, and 10^{-2}). Recordings started with the application of a blank stimulus (empty headspace bottle), followed by the odorant stimuli with rising odor concentration. After a complete sensillum recording the valve was flushed with air over night, in order to remove residual odorants in the valve.

To determine the rise time of the odorant stimulus (Figure 1A), we replaced the original stainless steel inlet needle of the PID by a 24.5 mm long glass needle in order to reduce low pass filtering of the odorant due to absorption at the inlet needle.

Data Analysis

Spike sorting: Spikes were sorted with Spike2 and then reviewed manually. The data was analyzed with custom scripts in R (version 3.1.1). The spike time was defined as time when the spike amplitude reached its maximum. Original spike time data is available in Data S1.

First spike latency: The time between the arrival of the stimulus at the fly antenna and the first recorded spike after stimulus arrival was taken as the first spike latency. In cases where the stimulus did not elicit a response, the first spike latency is the latency of the first spontaneously generated spike after stimulus onset. The colored points in Figure 2A show the median first spike latencies over 10 responses for each recorded neuron.

Spike rate: In order to facilitate the comparison between spike rate and first spike latency, we used the inverse spike rate, the interspike interval (time between two spikes n and n + 1). The minimum interspike interval was determined for a 500 ms window after the first spike. The colored points in Figure 2C show the median interspike interval over 10 responses for each recorded neuron.

Trial-to-trial jitter of first spike latency: The trial-to-trial jitter of the first spike latency was quantified as the standard deviation of the first spike latencies across 10 stimulus repetitions.

Neuron-to-neuron jitter of first spike latency: The neuron-to-neuron jitter of the first spike latency was quantified as the standard deviation of the differences between first spike latencies of the two simultaneously recorded neurons across 10 stimulus repetitions.

Pooling: For calculating the stimulus detection accuracy d_a and for neural model simulations, all recordings for a given olfactory receptor neuron type (OR22a or OR59b neurons) were pooled and trials were randomly selected from that pool. Each pool consisted of at least 10 trials with 10 renditions each, resulting in at least 100 spike trains for any given combination of receptor neuron type, odorant and concentration. This pooling procedure is justified, because spikes are independent in olfactory receptor neurons (Kazama and Wilson, 2009).

Stimulus detection accuracy d_a: Detection accuracies were calculated in a similar way as described by (Jeanne and Wilson, 2015). For each d_a value the following procedure was performed: From the pool of all measurements 40 combinations of n neurons were randomly selected (with n being the number given in the Figures). For each combination, all spikes in the specified integration time windows were summed up in order to obtain spike count distributions over the 40 combinations. For the distribution of odor-evoked spike counts, the window latency and length is given in the respective Figures. For the distribution of spontaneous spike counts all possible non-overlapping windows of given length in the 3 seconds before stimulus trigger were used. Using the mean and standard deviation of those distributions, d_a was calculated as the difference of means divided by the root-mean-square standard deviation:

$$d_a = \frac{\mu_{evoked} - \mu_{spontaneous}}{\sqrt{\frac{1}{2}\left(\sigma^2_{evoked} + \sigma^2_{spontaneous}\right)}}$$

This procedure was repeated 50 times in order to obtain mean and standard deviation of detection accuracy.

We used d_a > 5 as threshold for reliable separation of odorant-evoked and spontaneously generated spikes. To estimate the false-positive rate at d_a > 5 we calculated 315 spike count distributions for d_a values between 4 and 5 across all recordings. The overlap between spike count distributions of odor-evoked and spontaneous spikes was 0.08 ± 0.36 % (mean ± SD). Thus, at d_a > 5, the false-positive rate is less than 1%.

Spike probability: The spike probability during a sliding, 1 ms-wide window (rectangular kernel, 0.04 ms step size) was determined over 10 stimulus repetitions. This spike probability was then averaged over all recordings of the same receptor neuron type, odorant and concentration (Figure 1C, Figure S1C).

Statistical analysis: Statistical significance of differences in first spike latency (Figure 1D, Figure S2), first spike latency jitter (Figure 1A, Figure S2), spike rate (Figure 1F, Figure S2), integration time to d_a > 5 (Figure 2D) and minimum latency to d_a > 5 (Figure S4) across different concentrations was assessed using a Wilcoxon signed rank test and a *post-hoc* Holm-Bonferroni correction (* p<0.05, ** p<0.01, *** p<0.001).

Classification by threshold (Figure 3C): We used a threshold to predict odorant identity based on the difference in first spike latencies (Figure 3A) or the difference in minimum interspike intervals (Figure 3B) between OR22a and OR59b neuron responses. All possible such differences in the training set (80% of the data) were used to determine a single threshold that classified both odorants across all concentrations best. The threshold classifier was then applied to the test set (the remaining 20% of the data) and the percentage of correct classifications was calculated (classification rate). A classification rate of 50 % corresponds to chance classification. The process was repeated for 100 randomly selected training and test sets.

Modelling/Simulations: To classify odorants based on measured receptor neuron responses, a network of 5 spiking neurons, which was inspired by the olfactory system of the fly (Figure 3D, 3E, Figure S5), was simulated using the Python-based simulator Brian2 (integration using Euler method with dt = 25 µs). The network consists of two model Kenyon cells (KC_X and KC_Y) that receive weighted input from two model projection neurons (PN_X and PN_Y) and one inhibitory neuron (I). The inhibitory neuron is excited by projection neurons and inhibits Kenyon cells (feed-forward inhibition). As input to the projection neurons, recorded spike trains of 23 OR59b and 8 OR22a neurons were selected randomly from the pool of all recordings. Odorant classification was correct when methyl butyrate induced a spike response in KC_X but not in KC_Y, and when ethyl acetate induced a spike response in KC_Y but not in KC_X. Classification rate was calculated as the percentage of correct classifications during 100 simulation runs for each odorant. All neurons were simulated as leaky integrate-and-fire (LIF) neurons with conductance-based synapses (without synaptic transmission delays) and conductance transients (EPSG) described by an alpha function (Yim et al., 2014). The membrane potential V_m is given by:

$$C_m \frac{dV_m(t)}{dt} = -G_{syn}(t)(V_m(t) - V_{rev}) - G_l(V_m(t) - V_{res})$$

When the threshold was reached, V_m was reset and kept at the resting potential V_{rest} for the duration of the refractory period. The synaptic conductance G_{syn} is the sum of the presynaptic spikes convolved with the alpha function kernel (t_k denotes the spike time of the kth presynaptic neuron):

$$G_{syn} = \sum_k g_{syn}(t - t_k)$$

$$g_{syn}(t) = \begin{cases} J\frac{t}{\tau}e^{1-\frac{t}{\tau}} & if \quad t \geq 0 \\ 0 & if \quad t < 0 \end{cases}$$

The parameters of the neurons were chosen according to the literature (Table S1).

Note, that for the sake of simplicity we omitted several properties of the *Drosophila* olfactory system. For example, 1) we did not include laterality in our model. However, in contrast to most other insects, in *Drosophila*, olfactory receptor neurons project bilaterally to both antennal lobes (Couto et al., 2005), and compared to contralateral receptor neurons, spikes of ipsilateral receptor neurons arrive 0.8 ms earlier at projection neurons, release more transmitter and can evoke 2.5 ms shorter first spike latencies in projection neurons (Gaudry et al., 2013). 2) We restricted the inputs to Kenyon cells to two projection neurons only. However, in *Drosophila*, their number varies from 2 to 12 (Caron et al., 2013; Gruntman and Turner, 2013). 3) Our model Kenyon cells require inputs from 2 projection neurons in order

to generate spikes. However, in *Drosophila* some Kenyon cells can even respond to the input of a single projection neuron (Gruntman and Turner, 2013). 4) We did not implement Kenyon cell driven feedback inhibition onto Kenyon cells themselves (Lei et al., 2013; Lin et al., 2014; Papadopoulou et al., 2011).

Supplemental References

Caron, S.J.C., Ruta, V., Abbott, L.F., and Axel, R. (2013). Random convergence of olfactory inputs in the *Drosophila* mushroom body. Nature *497*, 113–117.

Couto, A., Alenius, M., and Dickson, B.J. (2005). Molecular, anatomical, and functional organization of the *Drosophila* olfactory system. Curr. Biol. *15*, 1535–1547.

Münch, D., and Galizia, C.G. (2016). DoOR 2.0 - Comprehensive mapping of *Drosophila melanogaster* odorant responses. Sci. Rep. *6*, 21841.

Szyszka, P., Demmler, C., Oemisch, M., Sommer, L., Biergans, S., Birnbach, B., Silbering, A.F.A.F., and Galizia, C.G.G. (2011). Mind the gap: olfactory trace conditioning in honeybees. J. Neurosci. *31*, 7229–7239.

Turner, G.C., Bazhenov, M., and Laurent, G. (2008). Olfactory representations by *Drosophila* mushroom body neurons. J. Neurophysiol. *99*, 734–746.

Yim, M.Y., Kumar, A., Aertsen, A., and Rotter, S. (2014). Impact of correlated inputs to neurons: modeling observations from in vivo intracellular recordings. J. Comput. Neurosci. *37*, 293–304.